Application of computer vision techniques to estimate surface roughness on wood-based sanded workpieces.

[Accepted manuscript]

F. Iglesias[a], A. Aguilera[b], A. Padilla[a], A. Vizan[c], E. Diez[a,*]

a Department of Mechanical Engineering, Universidad de La Frontera, Temuco, Chile.

b Instituto de Bosques y Sociedad, Universidad Austral de Chile, Valdivia, Chile.

c Department of Mechanical Engineering, Escuela Técnica Superior de Ingenieros Industriales, Universidad Politécnica de Madrid, Madrid, España.

* Corresponding author. E-mail address: eduardo.diez@ufrontera.cl (E. Diez).

Please cite this article as:

F. Iglesias, A. Aguilera, A. Padilla, A. Vizan, E. Diez, Application of computer vision techniques to estimate surface roughness on wood-based sanded workpieces, Measurement (2024), doi: https://doi.org/10.1016/j.measurement.2023.113917

Abstract

In the wood industry, surface inspection post-sanding is critical during the final production stages. This inspection relies on subjective assessments made by operators due to the challenges of adapting traditional measuring techniques to industrial environments. This study introduces an innovative artificial vision approach for the in-line inspection of surface roughness applied to wood and wood-based products in highly automated manufacturing systems. The procedure is based on extracting features from the grey-level co-occurrence matrix in images processed with edge-detection algorithms. Images are derived from photographs of sanded medium-density fibreboard, and models predicting surface roughness were formulated and compared with direct measurements using a stylus profilometer and a confocal microscope. Results showed that the most effective algorithm-feature combination was Roberts and Uniformity of Energy, with consistent performance for different roughness parameters. This approach can improve quality control and extend to a broader range of materials and applications.

Keywords: wood-based products; finishing operations; artificial vision; stylus profilometry; confocal microscopy; roughness models.

1. Introduction

In the wood products manufacturing industry, it is necessary to continuously improve the quality of products and components by optimising the operations involved in the manufacturing process. Finishing operations are of great relevance in the definition of final quality, a stage in which it is essential to conduct a detailed inspection to detect manufacturing errors according to the product's dimensional, geometric, and surface finish specifications. In addition, developing emerging manufacturing systems that aim to automate finishing operations using industrial robots [1] brings new challenges in designing quality inspection technologies to operate in highly automated environments.

Inspecting the surface finish of a sanded wooden workpiece determines if the workpiece is accepted, rejected, or requires an additional operation. The surface finish will affect the adhesion force in applying coatings [2] and the user's perception of the product's final quality. Inspecting sanded workpieces is a critical task that is difficult to automate due to its multiparametric nature, which motivates, in the wood furniture industry, the inspection to be usually carried out through the subjective perception of the operator [3]. To quantitatively determine the quality of a surface, roughness measurement is used after an intermediate or final operation. However, using roughness measurement instruments in wood product manufacturing is infrequent due to the costs of purchasing measurement equipment, personnel training, measurement times, and the difficulties when measuring curved geometries if a contact stylus profilometer is used.

Additionally, evaluating the surface roughness of wood products is a complex procedure, and there still needs to be an accepted methodology for performing roughness measurements on wood [4]. The results of the surface roughness measurement in processed wood vary depending on multiple factors, some associated with the type of wood, type of cut, structural characteristics, operating conditions, the measuring instrument used, and the processing of the wood profile, a representation of the measured surface texture to which different filters are applied before the roughness parameters are calculated. So many factors increase the difficulty in determining the influence of the process on the roughness of the piece. In the case of homogeneous materials such as medium-density fibreboard (MDF), since there is no fibre orientation [5], there are more appropriate conditions to determine the influence of the operation on the surface quality, decreasing the variability in the roughness present in the sanded workpiece. However, it is recognised that the roughness might change for varying depths in MDF due to changes in density as a result of the MDF manufacturing process [6].

Gurau & Irle [4] reviewed methods to evaluate the wood surface roughness. Those approaches show that some researchers emphasise the elimination of cracks in the roughness profile, which are frequent in wood pieces, before calculating the amplitude parameters, thus improving the sensitivity of roughness to changes in operating conditions. This review also gathers different roughness measurement methods, from which it follows that conventional measuring instruments, commonly used in the laboratory, can be categorised as contact measuring equipment (i.e., stylus profilometer, atomic force microscope), and contactless measuring equipment (i.e., autofocus roughness meter, white light interferometer, confocal microscope). These instruments measure surface texture parameters associated with a profile or a surface according to ISO Geometrical Product Specifications (GPS) standards.

There is currently no agreement about the preference for using contact or contactless methods to evaluate the surface finish of wood products. Magoss et al. [7] studied the use of confocal microscopy in the evaluation of the surface roughness of wood, obtaining that the mean of the parameters R_a, R_q, R_z, R_k and R_{vk} were close to the parameters calculated from data measured with a stylus profilometer. In the case of the R_{pk} parameter, the values measured with the confocal microscope turned out to be higher than when using the conventional stylus profilometer due to the higher resolution available in the microscope, which does not apply a mechanical filter as the stylus tip does (Figure 1), and when anomalous values are recorded by the sensor light saturation, reported by Caja García et al. [8]. However, Magoss et al. [7] concluded that the observed differences could be corrected by applying filters and eliminating artificial peaks, proving that confocal microscopy is an adaptable method for measuring the surface quality of wood pieces.

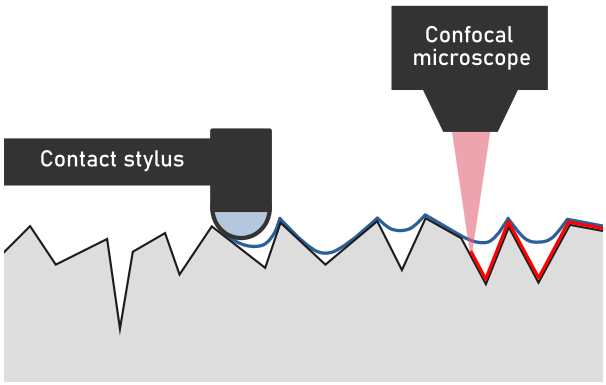

Figure 1. Stylus profilometer and confocal microscope behaviour when measuring a surface.

Among the instruments mentioned above, only the stylus profilometer is feasible to use at an industrial level due to its costs and measurement times. However, its use is limited to flat surfaces. To develop automated inspection systems, it is necessary to test fast, non-conventional techniques for evaluating wood parts that can be applied in the industry. Liu et al. [9], who reviewed cutting tool failure diagnostic procedures by monitoring the surface texture of machined metal parts, pointed out the advantages of evaluating surface roughness through machine vision-based inspection systems, which take measurements faster and without scratching the surface. On the other hand, machine vision-based techniques proved to be more convenient and consistent than manual inspections in evaluating surface roughness.

Techniques based on two-dimensional images allow fast and low-cost results, apply to surfaces that are difficult to measure using conventional instruments due to geometric or dimensional factors of the parts, and allow for an easy integration into automated systems, inspection stations, or intelligent systems [9]. In recent years, there has been a significant development in machine vision techniques to inspect the quality of parts [10]. Regarding surface roughness, tests have been carried out using algorithms that consider direct calculations on the pixels of a digital image, applying filters, statistical techniques, and machine learning algorithms through artificial intelligence algorithms [11].

In the literature, there are examples of different techniques to assess the surface quality of parts from images, such as the extraction of roughness parameters from the grey-level histogram [12], the measurement of the intensity of light reflected by the surface in MDF boards [13] or the roughness estimation from analysis of light intensity differences in wood workpieces [14]. A method that showed a high correlation between the features extracted from the images and the standardised roughness evaluation parameters corresponds to the one proposed by Ghodrati et al. [15], who used image edge detection algorithms to estimate the roughness of plastic parts. Other examples of roughness estimation are those proposed by Lu et al. [16], who applied Laplacian-based edge enhancement on surfaces of casting components, Koblar & Filipič [17], presented the design of an online algorithm that applies an FFT filter and extracts features, which are used in a machine learning algorithm to predict roughness, and Kilinçarslan et al. [18] used an artificial neural network and random forest algorithm to predict roughness in heat-treated spruce wood surfaces.

Another technique applied in studies that seek to determine roughness from images is obtaining features from the grey-level co-occurrence matrix (GLCM), which measures

the frequency of grey-level patterns between neighbouring pixels in an image. The first use based on the GLCM associated with the roughness evaluation was made by Gadelmawla [19]. Co-occurrence matrix-based techniques to measure roughness may vary depending on the specific material and the roughness range evaluated, which is why a previous calibration step is necessary [20]. Moreover, there are studies in the literature on using features extracted from the GLCM in the training of neural networks to estimate surface roughness, like the works done by Joshi & Patil [21] and Kumar et al. [22].

Some investigations have focused on developing deep learning models, such as using a convolutional network to evaluate roughness in machined parts processed by turning and milling [23] and in assessing roughness and defects [24]. Rifai et al. [25] estimated surface roughness and identified chatter vibration using vision-based deep learning. Lu et al. [26] developed a deep learning model combined with simulation data to recognise surface roughness in milling; Bhandari et al. [27] implemented a transformer-based deep learning architecture to classify surface roughness using sound and cutting force signals in end-milling; and He et al. [28] developed a theoretical and deep learning hybrid model to predict the surface roughness of diamond-turned polycrystalline materials. However, machine learning-based techniques, such as those mentioned above, require a large amount of data in the training stage and bring difficulties that need attention, such as model overfitting and out-of-range prediction problems.

Based on the review outlined here, there is still no suitable method to evaluate the roughness of wood pieces using machine vision. To contribute to the advancement of the study of artificial vision techniques to inspect surfaces and, at the same time, compare different instruments for measuring roughness on sanded wood pieces, in this work, a novel method is developed to estimate the surface roughness of wood pieces based on combining GLCM and edge detection algorithms to obtain roughness parameters from photographic images. The proposed method is conceived to apply to in-line roughness inspection in highly automated sanding and polishing robotised stations.

2. Methodology

Automating sanding processes with industrial robots requires the development of fast and reliable inspection systems, which allow roughness to be measured with sufficient precision. The proposed method based on artificial vision requires previous calibration against known input values of roughness. In this study, the calibration is carried out with state-of-the-art instruments: contact measurement with a stylus profilometer and

contactless measurement with a confocal microscope. The calibration process begins with the photographic capture of the surface of the pieces. These images can be acquired from specimens taken from the product across its different sanding stages. The images are transformed to greyscale and then processed with five edge detection algorithms. Then, the GLCM is calculated for each image resulting from the above processing, including the original greyscale image, and five features are obtained from the matrix. With the roughness parameters and the features of the images, the best models are fit and selected, making it possible to estimate the roughness from new images. Next, the materials and methods considered in this study are described in detail.

2.1 MDF sanded workpieces

Sanded MDF workpieces, 180 x 110 x 15 mm^3, were used. An aerosol polyurethane coating was applied to the lower surface of the specimens for correct attachment with the vacuum fixture.

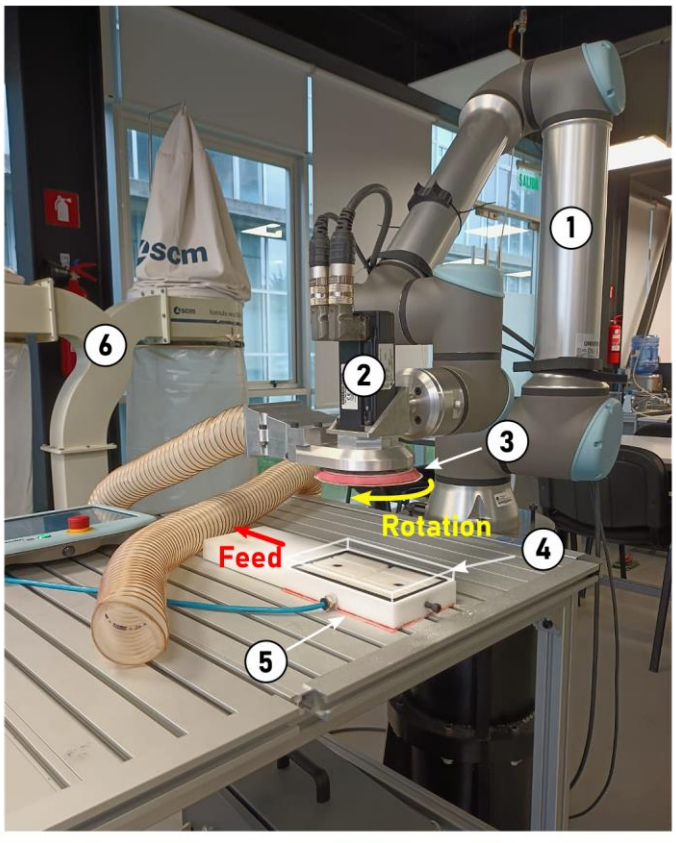

Figure 2. Robotic sanding station in which the MDF specimens were prepared.

Two experimental robotic sanding campaigns were carried out with the same operating conditions: one for obtaining estimation data (15 workpieces) and the other one for validation data (9 workpieces). The sanding process was carried out with a sander of in-house design [1], driven by a servo motor mounted on the flange of a collaborative robot UR10e (Figure 2). A force of 20 N was applied to the specimen perpendicular to the feed direction, controlled by the collaborative robot; a rotating speed of 2000 min^{-1} in the servomotor; and a feed speed of 0.02 m/s, defined through a linear movement of the sanding pad, parallel to the surface of the specimen. The three types of circular sandpaper were 3M™ Cubitron™ II Hookit™ 127 mm diameter, with perforations for particle suction.

In both experimental campaigns, the total number of specimens was subdivided into three groups: the first was processed with coarse P80 grit size (one pass), the second with P120 (one pass), and the third was sanded with two passes, one with P120 and the other, finer, with P240, considering the need to apply incremental sanding when using finer grits. In the sanding tests, the minimum number of passes was considered to avoid the variations in density present in MDF boards at different depths [29].

2.2 Roughness measurement

To measure roughness, three measurement methods have been considered. One is a classic measurement by contact, a stylus profilometer, and two are optical, one based on a confocal microscope, which provides a high-precision digital definition of the surface geometry of the part, and another based on computer vision, where a general evaluation of the image is made. These methods exhibit advantages and limitations related to the nature of their measurement principles. Contact profilometer measurement is fast, reliable, robust, and can be applied to any part size. The confocal measurement is slow and limits the dimensions of the piece to be explored, but the high precision of the geometric model obtained provides excellent flexibility for the measurement and the definition of any normalised roughness parameter. It also performs a superficial scan instead of a linear scan. Vision-based measurement is fast and easy to incorporate into production lines, although it can have limited accuracy. The system proposed in this work is based on this type of measurement.

In this study, the confocal evaluation of the roughness will be intercompared with the measurement by contact of the workpiece. At the same time, the normalised roughness

parameters obtained with these procedures will be intercompared with the parameters obtained by visual image processing.

To obtain a comprehensive description of surface roughness, it is necessary to use more than one roughness parameter, even if the part surface is homogeneous [30]. For this reason, five parameters were selected based on the physical information provided by the sanding operation: the arithmetic mean height R_a, the maximum height R_z, the mean peak height R_p, the mean profile element spacing R_{sm}, and the skewness R_{sk}, according to ISO 21920-2.

The measurements were made in the central area of the specimen in the feed direction of the rotating sanding pad (see Figure 2).

2.3 Roughness parameters

The surface roughness parameters are defined by the ISO 21920-2 [31] standard, published in December 2021, which replaces the ISO 4287, ISO 13565-2 and ISO 13565-3 standards and implements some modifications in the stages of the profile processing and the way to calculate some roughness parameters. The new standard also increases the available parameters to describe surface roughness.

For profile processing, the new standard considers the application of three filters in the order shown in Figure 3. Once the mechanical profile is obtained with the stylus tip, an S profile filter is applied to eliminate the small lateral scale components (short wavelength), with nesting index N_{is}, to obtain the primary surface profile. Then, operation F is applied to eliminate the profile form, using an association method and element (for example, a polynomial fit of order n by least squares), a filter L, which removes the large lateral scale components (long wavelength), with nesting index N_{if}, or a combination of stages. Once the form has been subtracted from the profile, the primary profile P is obtained, to which a filter L or a filter S with nesting index N_{ic} is applied to get the roughness profile R or the waviness profile W, respectively.

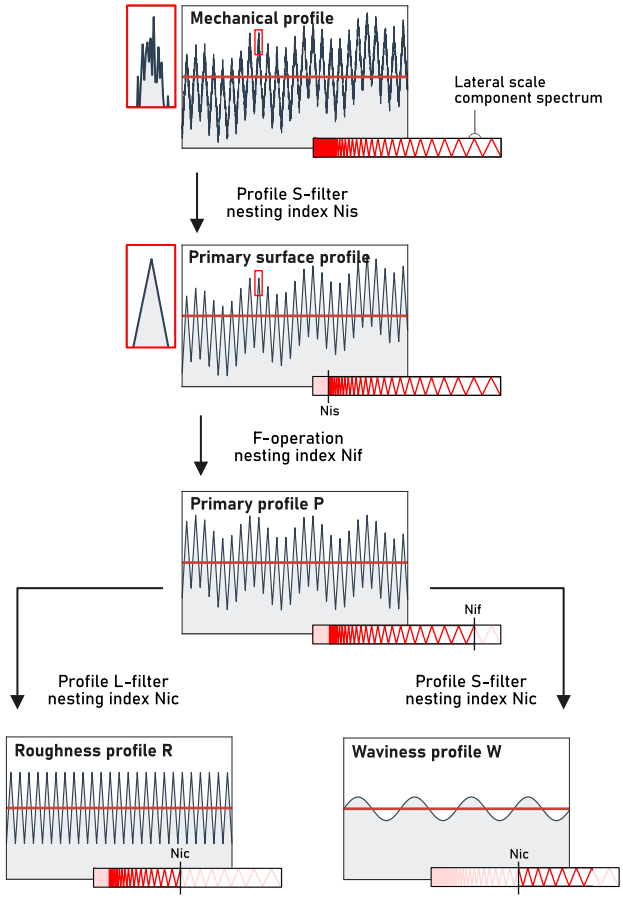

Figure 3. Profile processing scheme based on ISO 21920-2.

In the new standard, the classification of roughness parameters changes. Previously, the amplitude parameters of mean values were an average of the calculation at each sample length (now section length); in the new standard, some of these parameters are calculated directly from the evaluation length. The parameters selected in this work are defined below, based on the ISO 21920-2 standard, and have been adapted for digital implementation. In addition, the changes observed in the new standard are mentioned.

Arithmetic mean height (R_a)

The R_a parameter is considered since it is a good representation of the distribution of profile deviations from the mean line, and its use is widespread in the industry. The height parameter R_a does not experience changes in the renewal of the standard; it was previously calculated as the average of R_a for each section; now, it is obtained directly from the evaluation length, which is mathematically equivalent in the case of this parameter.

$$R_a = \frac{1}{n}\sum_{i=1}^{n}|z_i|, \quad (1)$$

where n is the number of points of the roughness profile, and z_i is the height of the i-th point of the profile.

Skewness (R_{sk})

The skewness is a factor that could influence the uniformity of the coating, varnish or paint layers and could be indicative of the surface geometry of the sanding disc. It is also calculated directly from the evaluation length as it is a height parameter, so there are differences in the result compared to the previous standard, which applies it to each section length and then calculates the average.

$$R_{\mathrm{sk}} = \frac{1}{R_{\mathrm{q}}^3}\frac{1}{n}\sum_{i=1}^{n} z_i^3, \tag{2}$$

where R_q, the root mean square height, is obtained according to Equation 3.

$$R_{\mathrm{q}} = \sqrt{\frac{1}{n}\sum_{i=1}^{n} z_i^2} \tag{3}$$

Maximum height (R_z)

This parameter is related to the regularity of the sanding process, and it makes sense to associate it with an evaluation of R_a. According to ISO 21920-2, R_z is a feature parameter defined as the mean of the distance between the maximum peak height (z_{ph}) and pit depth (z_{vd}) of each section. Previously, an independent R_z was obtained for each section length (l_{sc}), corresponding to the profile evaluation length divided by the number of sections.

$$R_{\mathrm{z}} = \frac{1}{n_{\mathrm{sc}}}\sum_{i=1}^{n_{\mathrm{sc}}}\left(\max_{j\in N_{\mathrm{p},i}}\left(z_{\mathrm{ph},j}\right) + \max_{j\in N_{\mathrm{v},i}}\left(z_{\mathrm{vd},k}\right)\right), \tag{4}$$

where:

n_{sc} is the number of profile sections.

$N_{p,i} = j = 1,2,\dots,n_p | (i-1)l_{sc} \le x_j < i \cdot l_{sc}$;

$N_{v,i} = k = 1,2,\dots,n_v | (i-1)l_{sc} \le x_k < i \cdot l_{sc}$;

n_p is the number of the profile peaks;

n_v is the number of the profile pits;

x_j is the position of the j-th peak on the X-axis;

x_k is the position of the k-th peak on the Y-axis.

Mean peak height (R_p)

This parameter complements the previous one and reveals the shape of the sandpaper grain and its distribution, as well as the number of passes made during sanding. It is a feature parameter indicating the average of the maximum height of each section. In this case, the modification is analogous to the parameter R_z.

$$R_{\mathrm{p}} = \frac{1}{n_{\mathrm{sc}}} \sum_{i=1}^{n_{\mathrm{sc}}} \max_{j \in N_i} \left(z_{ph,j} \right), \tag{5}$$

where $N_i = j = 1,2, \ldots, n_p | (i-1) l_{sc} \leq x_j < i \cdot l_{sc}$

Mean profile element spacing (R_{sm})

This parameter can indicate the distribution of the abrasive in the sandpaper and how the process has been carried out. It is a parameter based on the profile elements, indicating the average spacing between each element in the evaluation length. It is worth mentioning that for correct discrimination of the profile element in the digital implementation, it is recommended to use the code developed by Seewig et al. [32]

$$R_{\mathrm{sm}} = \frac{1}{n_{\mathrm{pe}}} \sum_{i=1}^{n_{\mathrm{pe}}} X_{\mathrm{s},i}, \tag{6}$$

where n_{pe} is the number of profile elements and $X_{s,i}$ is the spacing of a profile element.

2.4 Stylus profilometer

A Mitutoyo SJ-310 stylus profilometer with a 5 μm stylus tip radius was used. Three measurements were made in the centre of each specimen in the direction of the feed rate, using a template to ensure measures in the same specimen area, as shown in Figure 4. In every case, the evaluation length was 12.5 mm.

For the processing of the profile, the following steps were considered: a Gaussian S filter was applied to the mechanical profile with $N_{is} = 0.008\ mm$; then, in operation F, a fit and subtraction of a polynomial of degree 6 was performed using least squares [33]; and finally a Gaussian L filter with $N_{ic} = 2.5\ mm$ was applied to obtain the roughness profile. Due to the low presence of cracks in the MDF specimens, a robust Gaussian regression filter was not considered. Both the processing of the profile and the calculation of the parameters were carried out in MATLAB R2023a [34].

The uncertainty in the roughness parameters was estimated by grouping the three measurements of each specimen, calculating the 95% confidence intervals in Student's t-distribution. The time required for measuring each workpiece is close to six minutes.

Figure 4. The equipment used for roughness characterisation.

2.5 Confocal microscope

Measurements were made using a Zeiss LSM 700 confocal microscope, Axio Imager 2, with an Epiplan-Apochromat 10x/0.4 DIC M27 C objective, fluorescent contrast method with 405 nm wavelength laser light, at 4.0%, using a 0.29 AU pinhole. A unidirectional frame scan was performed with 968.15 ms, obtaining an image of 10240 x 512 px, equivalent to 12.80 mm x 640.17 µm, with a variable number of layers depending on the roughness of the MDF specimen, each layer separated at a height of 1.00 µm.

The Zeiss Zen Black 2012 software was used for image acquisition, and the Confomap Mountains software [35] was used to visualise and obtain roughness parameters. As shown in the diagram of Figure 5, three lines were drawn along the surface to extract roughness profiles; later, the same configuration used with the profiles measured with the stylus profilometer was applied for profile filtering and parameter calculation. Uncertainty was estimated equivalent to using the contact method, with 95% confidence intervals in a Student's t-distribution. The time required for measuring each specimen depended on the number of layers, taking an approximate maximum of 45 minutes per workpiece.

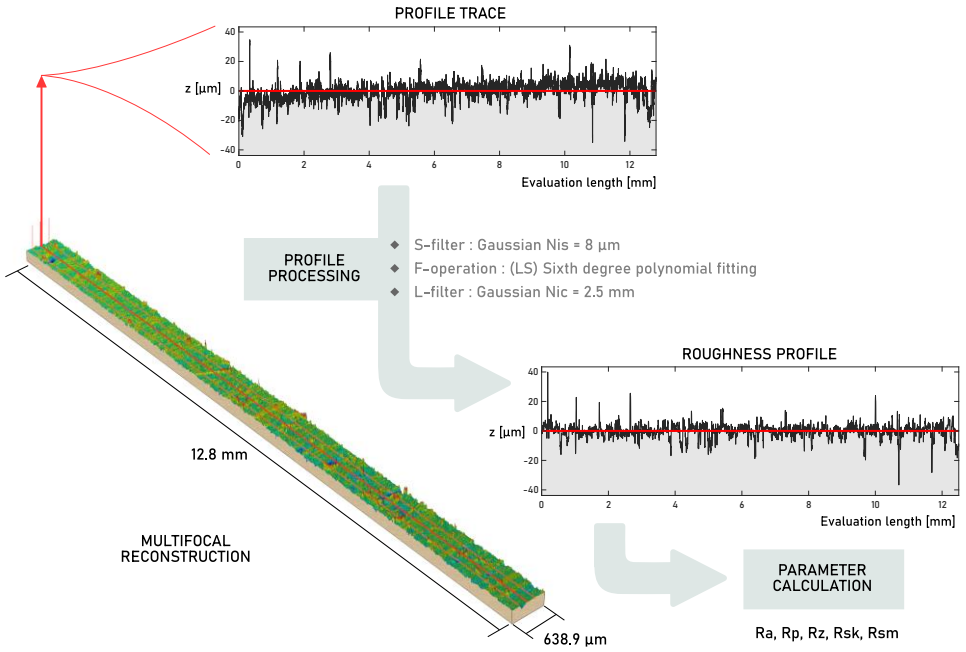

Figure 5. Scheme for obtaining profiles from the reconstructed image with the confocal microscope.

2.6 Artificial vision

Image acquisition was performed in a space with lighting controlled by a side LED (assembly of 8 LED strip with diffuser plate, 45 mm long, luminous flux of 280 lm, temperature of colour of 3000 K, incidence angle of 70-80°), with a SONY STL-A58 camera with DT 3.5-5.6/18-55 SAM II lens, 30 mm focal length, F14 aperture, exposure time 10 s, ISO 100, so that the image plane was parallel to that of the sanded surface, at a physical distance of 400 mm between the lens and the specimen, as shown in Figure 4.

After the capture, the images are cropped in the central area of the MDF sample with a size of 78 x 676 px, equivalent to approximately 4.5 x 39 mm^2. Image processing consists of three stages. The first stage consists of the application of five edge detection algorithms to the greyscale image (Roberts, Sobel, Prewitt, Laplacian and Laplacian of Gaussian); in the second stage, the co-occurrence matrix is obtained for each one of the images; and in the third, five features are calculated from the matrix: Uniformity of Energy, Contrast, Homogeneity, Autocorrelation and Entropy. Image processing was implemented in Python 3.8 with the OpenCV library and GLCM feature extraction in MATLAB R2023a.

Stage 1. Edge detection algorithms

Edge detection helps detect surface marks (roughness) where the light reflection will differ. In an image, an edge is defined as a significant local change in the light intensity of a point concerning its surroundings. This implies the accomplishment of two criteria: the shift in intensity must be relevant and, at the same time, be delimited [36]. However, in this study, edge detection algorithms are considered as a method to enhance the marks that determine the surface quality and reduce the influence of the change in ambient light.

Edge detection algorithms usually consider three steps:

- Filtering to eliminate noise that can affect the image.
- Enhancement to facilitate edge detection based on intensity changes around a specific pixel.
- Detection, in which a threshold criterion is used to discern between the points that are edges and those that are not.

Since this work seeks to evaluate the roughness of a surface, it will only focus on the enhancement stage because applying a filter or a threshold could reduce the relevant information that describes the roughness. Five enhancement algorithms are analysed, of which three are based on the first derivative of the image intensity (Roberts, Sobel and Prewitt) and two on the second derivative (Laplacian and Laplacian of Gaussian). The first derivative shows the rate of change in intensity, while the second highlights the points where the rate of change varies, reducing the occurrence of highlighted edges. The derivatives are approximated through differences using convolution masks according to the equations presented in Appendix 1 [36].

Stage 2: GLCM

The grey-level co-occurrence matrix, also known as GLCM, is a second-order statistical technique applied to digital images in greyscale that estimates the probability of a spatial relationship between two pixels, a reference pixel and another one displaced by $d = (\Delta x, \Delta y)$. From an image I, of $n \cdot m$ px, a square matrix is obtained whose dimension varies according to the number of grey levels of the image, defined in Equation 7.

$$\boldsymbol{M}_{\mathbf{c}}(i,j) = \sum_{x=1}^{n} \sum_{y=1}^{m} \begin{cases} 1, & \text{if } I(x,y) = i \text{ and } I(x+\Delta x, y+\Delta y) = j \\ 0, & \text{otherwise} \end{cases} \tag{7}$$

The co-occurrence matrix M_c is added with its transpose, obtaining a symmetric matrix, which is then normalised, as shown in Equation 8.

$$\boldsymbol{M}_{\mathbf{cn}} = \frac{1}{2 \cdot \sum M_{\mathrm{c}}[i,j]} \left(\boldsymbol{M}_{\mathbf{c}} + \boldsymbol{M}_{\mathbf{c}}{}^{T} \right) \quad (8)$$

In this work, a normalised co-occurrence matrix is considered with a maximum of 8 levels and a displacement of $d = (1.0)$, perpendicular to the sanding marks that follow the direction of rotation of the sanding pad (Figure 2).

Stage 3. Calculation of features

In 1973, Haralick et al. [37] developed a set of 14 texture features intended to classify images based on the spatial distribution of grey levels. The features calculated from the GLCM are obtained in this work according to the definitions of Haralick and Shapiro [38], presented in Appendix 1. Algorithms were implemented to calculate the five most used features in the literature, consisting of Uniformity of Energy (U), Contrast (C), Homogeneity (H), Correlation—Autocorrelation in this paper—(A) and Shannon Entropy (S).

2.7 Model estimation

From the measurements performed on the set of 15 MDF specimens, using the stylus profilometer and the confocal microscope, Bayesian linear models [39] were created for each roughness parameter with the different combinations of GLCM features and the detection algorithm applied to cropped images (including the case of images without edge detection processing). Bayesian linear regression models are chosen because, unlike simple linear regression models, they make it possible to obtain prediction intervals that consider uncertainty as a probability distribution associated with estimating the model parameters. Subsequently, with the remaining 9 specimens, the models were validated. The estimated models are assessed using the root mean square error (RMSE) computed for estimation and validation data. Finally, the combination of algorithm and feature with the lowest RMSE was chosen for the roughness parameters. The estimation of the models was performed in MATLAB R2023a considering all estimation data points.

3. Results and discussion

The dataset in this study, which includes roughness data measured with the confocal microscope and the stylus profilometer, and the corresponding photographic images of each sanding test, is available for the reader in [40].

3.1 Roughness evaluation

For an adequate analysis of the results, it is necessary to check if the identification of the micro geometric profiles (mechanical and optical) is equivalent and provides similar information for calculating the normalised roughness parameters.

Figure 6 shows the mechanical profile obtained with the roughness tester for specimens sanded with sandpaper of different grain sizes. As expected, smaller grain sizes give rise to profiles with smaller deviations from the zero line. It can also be observed that the profile distribution is highly symmetrical, which is attributable to the regular shape of the abrasive grain. In the collected profiles, no influence of the previous processes to which the piece has been subjected is observed.

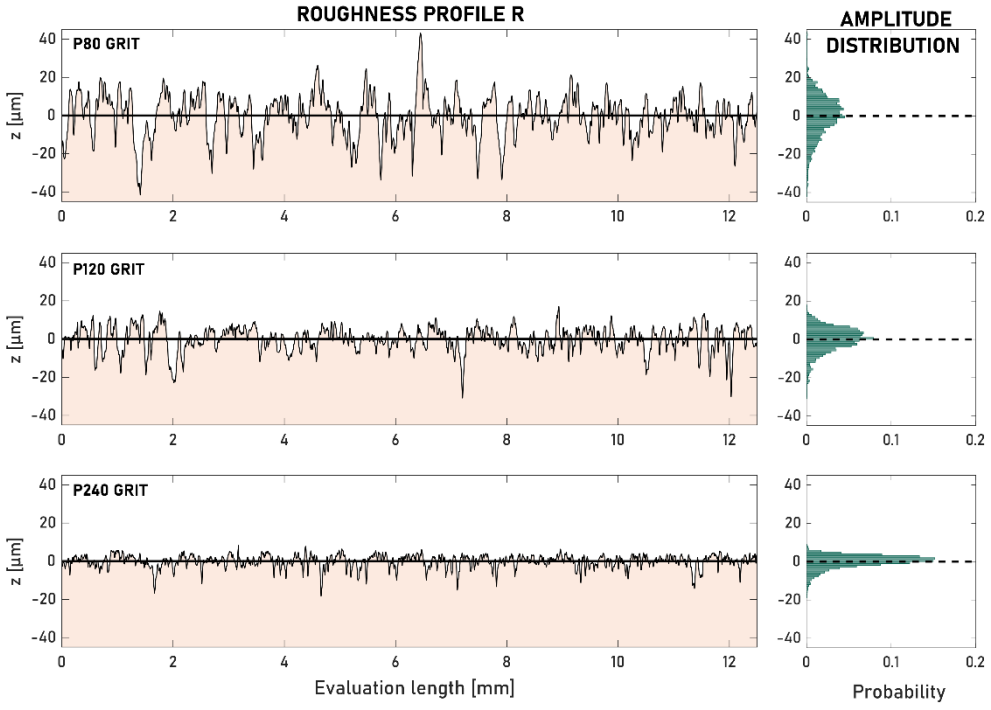

Figure 6. Roughness profiles obtained with the stylus profilometer and different grit sizes.

The confocal method identifies the micro-geometric surface according to the profiles obtained by the stylus profilometer (Figure 7). The distribution of the profile around the mean line is also very symmetrical and with a slightly more extended distribution, which confirms that the optical (confocal) method can obtain a profile with more resolution than a contact-based method (stylus). Similarly, smaller grain sizes result in narrower distributions of the profile deviation.

The characterisation of the surface microgeometry by both methods is similar, with greater resolution of the confocal method in the case of sanded MDF pieces.

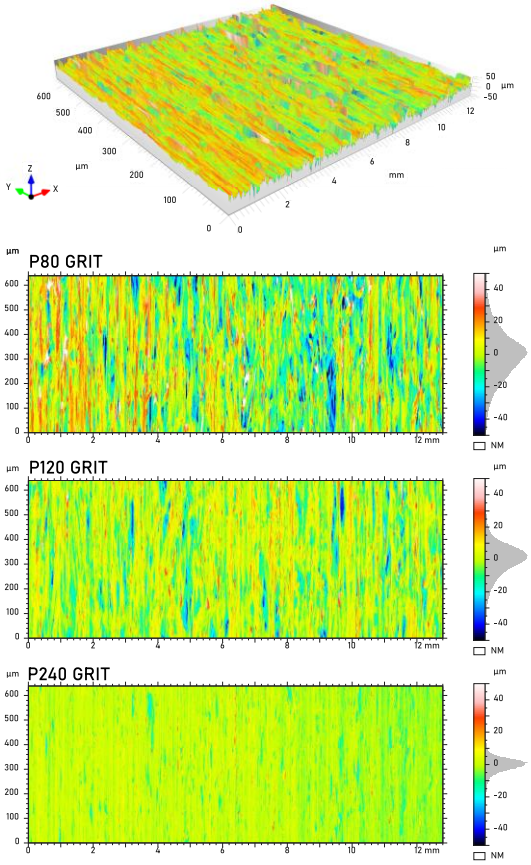

Figure 7: Examples of images obtained with the confocal microscope on specimens sanded with different grit sizes.

To analyse the associated dispersion when measuring with the stylus and the confocal microscope, the roughness measurements for each estimation specimen were plotted in Figure 8. While there is a natural tendency to reduce roughness using finer sandpaper, it is realised that a specific grit size does not necessarily imply a particular roughness level. When performing rough sanding with P80 sandpaper, there is a higher dispersion of roughness than in finer sanding. The roughness distribution in Figure 7 represents all

points of the multifocal reconstruction, which is more representative of the roughness behaviour than a specific line in the image.

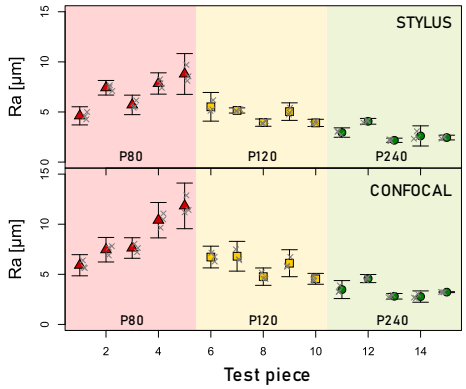

Figure 8: Confidence intervals (95%) of R_a for each specimen of the estimation tests.

Table 1 shows, for each grain size, the mean, median and standard deviation of R_a for the different confidence intervals. It is observed that the confidence interval ranges are reduced as sanding with finer grits; the same happens with the standard deviation of those ranges. It also follows that the confidence intervals of the parameters measured with the confocal microscope are usually larger than those obtained with the stylus profilometer, although similar results are obtained with the finest grain P240. A reduced dispersion is a good indicator of the instrument's performance. However, it must be considered that, due to the nature of the material, there is variability present on the surface.

Table 1. Summary of the confidence interval (95%) ranges of R_a for each grit size.

Grit size	Instrument	Mean [µm]	Median [µm]	Standard Deviation [µm]
P80	Stylus	2.28	1.95	1.03
	Confocal	2.94	2.45	1.08
P120	Stylus	1.32	0.73	0.99
	Confocal	2.13	2.17	0.75
P240	Stylus	0.88	0.57	0.66
	Confocal	0.88	0.81	0.64

In the graphs of Figure 9, a reduction in the magnitude of the roughness parameters can be seen as a finer grit is used (something similar occurs in the case of the confidence

intervals in the three height parameters: R_a, R_z, and R_p), which implies that the roughness parameters are not strictly independent in this particular operation. It can also be seen that with the confocal microscope, parameters of greater magnitude are usually obtained, especially in the case of the parameters R_z and R_p.

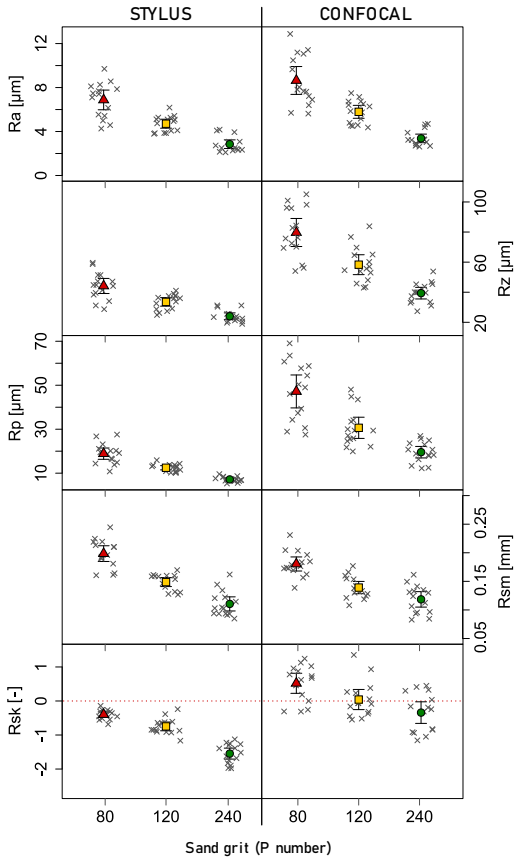

Figure 9. Roughness parameters measured with both instruments.

The intercomparison of the normalised roughness parameters calculated from not exactly equal profiles endeavours to determine if there is a correlation between these parameters.

To this end, a linear fit of the measurement data recorded by both techniques was carried out for each one of the roughness parameters obtained in the first 15 MDF workpieces, generating models defined by Equation 9, which were validated with the remaining nine workpieces (Figure 10). Table 2 shows the coefficients and some goodness of fit; note that RMSE is computed both with estimation and validation data.

$$R_{confocal} = w_0 + w_1 \cdot R_{stylus} \tag{9}$$

Table 2. Coefficients and goodness of fit of the models defined by Equation 9.

Roughness parameter (Confocal)	Interception w_0	Coefficient w_1	R^2 estimation data	RMSE estimation data	RMSE validation data
R_a **[µm]**	-0.2857	1.2933	0.95	0.60 µm	0.93 µm
R_z **[µm]**	-6.8871	1.9463	0.95	4.31 µm	8.12 µm
R_p **[µm]**	0.0458	2.5238	0.93	3.72 µm	5.41 µm
R_{sm} **[mm]**	0.0433	0.6730	0.83	0.01 mm	0.01 mm
R_{sk} **[-]**	0.7330	0.7349	0.47	0.40	0.17

The comparison shows that the confocal measurement has a higher resolution in the determination of R_z and R_p, since the range of the stylus is smaller than the one provided by the confocal method for the same measurements. This range is appreciably greater and about double. This demonstrates that the optical measurement better determines the pits and peaks of the profile. On the other hand, it is confirmed that the parameters R_z and R_p for a sanded MDF piece have a similar evolution, and therefore, they do not provide any additional information about each other as to the surface state of the workpiece.

As occurs with other processes, the parameters R_a and R_z (R_p) calculated by both methods are closely correlated, allowing an approximate conversion between them for the MDF sanding process.

The measure of the profile skewness expressed according to R_{sk} and the spacing defined by R_{sm} are very similar for both methods, which shows that these open surface characteristics can be evaluated without distinction by any of the methods.

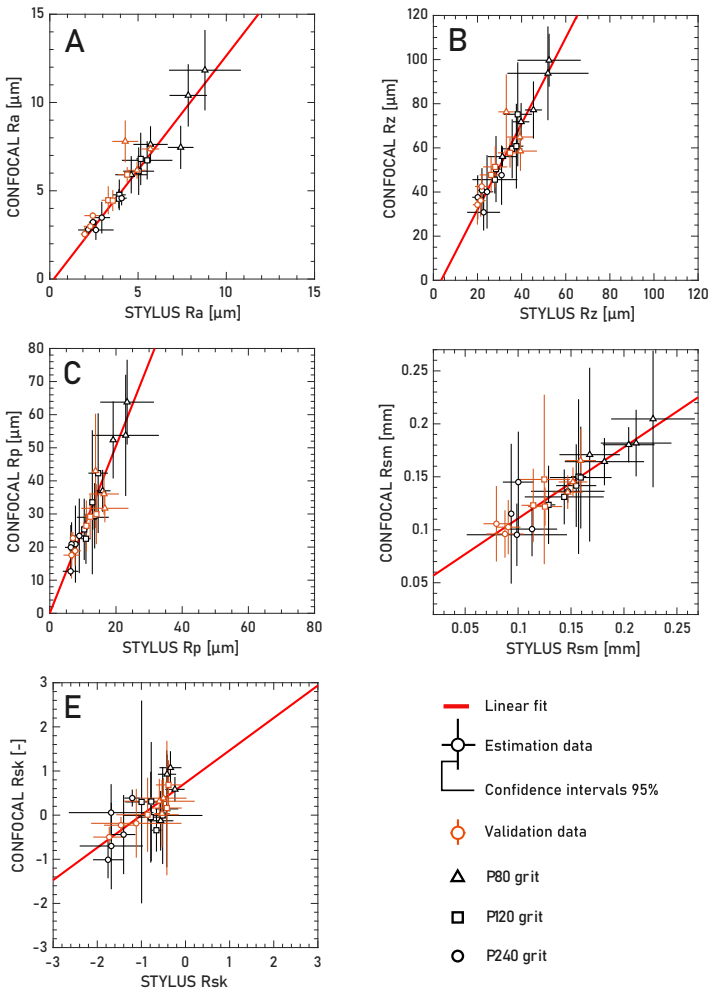

Figure 10. Comparison of roughness parameters obtained from measurements with the confocal microscope and the stylus profilometer.

3.2 Determination of surface finish through vision

Figure 11 presents cutouts of greyscale images that show the surface finish after the sanding operation using different grit sizes. The result is delivered to the right of each image after applying the various edge detection algorithms considered in this study. These images were captured to extract the features and fit the models. For expository reasons, we increased the brightness and contrast of the images, and a gradient map was applied so that the reader could better visualise the surface marks after processing with different edge detection algorithms. Like the Laplacian algorithm, the Roberts algorithm tends to obscure the marks but does not remove them. On the other hand, Sobel, Prewitt, and the Laplacian of Gaussian enhance markings to a greater degree.

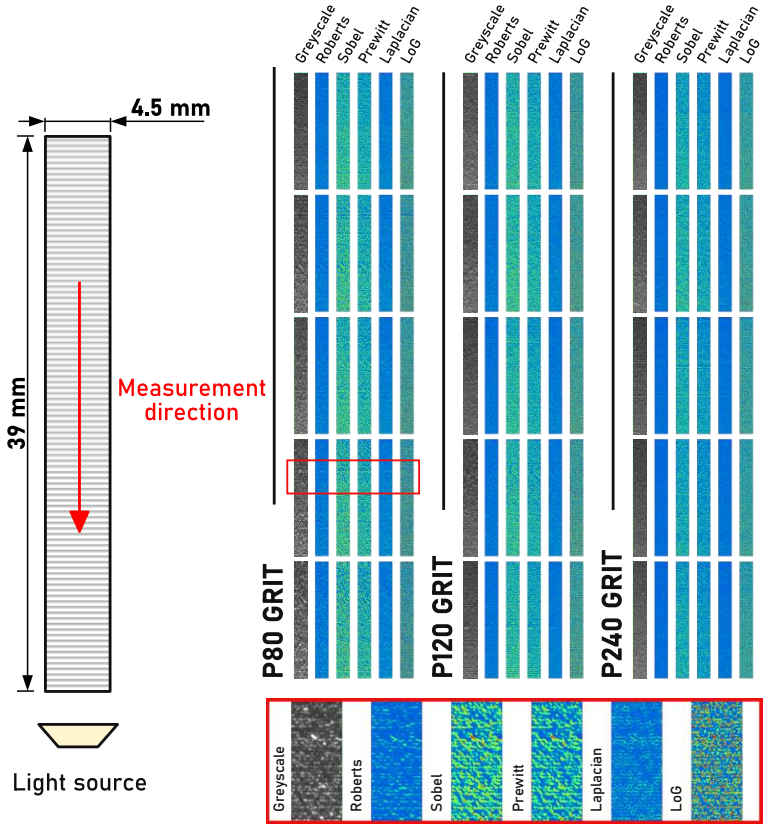

Figure 11. Images of MDF specimens sanded with different grit sizes and the result after applying the edge detection algorithms.

As specified in the methodology, for calculating the GLCM, a vertical displacement coinciding with the sanding feed was used to consider thereby the same measurement direction made with the stylus profilometer and the traces extracted from the image obtained with the confocal microscope (Figure 5).

Due to the difference observed between the contact and confocal measurement systems, models were made (Equation 10) comparing the features obtained when using vision algorithms with both measurement instruments separately. It is considered that, during the calibration stage, one of the two instruments will be selected, depending on availability, to perform calibration measurements on small-sized specimens made of the material to be processed.

The vision algorithms analysed showed different performances when estimating roughness. Tables 3 and 4 show some results for selected combinations of algorithm and feature in the estimation of the parameter R_a. The RMSE values in Table 3 are calculated from the fitted model between the stylus measurements and the features extracted from the photographed images processed with edge detection algorithms. Table 4 presents the RMSE values of the fitted model between the confocal microscope and image

features. Henceforth, the Roberts algorithm for edge detection and the Uniformity of Energy (U) feature were selected, which yielded the best RMSE results compared to all the other combinations. In addition, the mean absolute percentage error (MAPE) was calculated to evaluate the models. MAPE values, presented in Appendix 2, are consistent with the RMSE results.

Table 3. RMSE for stylus-based models (in μm).

	Uniformity of Energy (U)	Entropy (S)	Contrast (C)	Homogeneity (H)	Autocorrelation (A)
Original	1.16	1.07	1.16	1.37	1.84
Roberts	**0.66**	0.67	0.69	0.70	1.94
Sobel	1.62	1.29	0.91	1.32	2.32
Prewitt	1.43	1.18	0.86	1.22	2.14
Laplacian	0.91	0.92	0.89	0.94	1.49
LoG	1.93	1.74	1.54	1.89	2.71

Table 4. RMSE for confocal-based models (in μm).

	Uniformity of Energy (U)	Entropy (S)	Contrast (C)	Homogeneity (H)	Autocorrelation (A)
Original	1.60	1.42	1.69	1.94	2.17
Roberts	**1.03**	1.06	1.06	1.07	2.65
Sobel	2.19	1.82	1.33	1.80	3.28
Prewitt	1.96	1.70	1.28	1.69	3.05
Laplacian	1.41	1.44	1.37	1.41	2.26
LoG	2.51	2.22	2.11	2.44	3.76

A similar behaviour was observed with the parameters R_z and R_p. In the case of the R_{sm} parameter, the best result was Roberts with Entropy, although with a negligible difference from the result with Roberts and Uniformity of Energy. The parameter that performed worst was R_{sk}. To facilitate the comparison between the estimated models for each

parameter, it was deemed necessary to plot them maintaining the Roberts combination with Uniformity of Energy.

Figure 12 shows the models obtained by comparing the vision method with the stylus profilometer based on Equation 10. A Bayesian linear fit was used, and $\pm 2\sigma$ prediction intervals were obtained. Table 5 shows the model coefficients, the precision $\beta = \frac{1}{\sigma^2}$ and the coefficient of determination in the estimation R^2, together with the RMSE evaluations in the estimation and validation.

$$R = w_0 + w_1 \cdot v_{feature} \tag{10}$$

Table 5. Coefficients and goodness of fit of the models defined by Equation 10, using the stylus profilometer.

Parameter stylus	Interception w_0	Coefficient w_1	Precision β	R^2 estimation	RMSE estimation data	RMSE validation data
R_a [µm]	57.2507	-55.2224	2.67	0.90	0.61 µm	0.73 µm
R_z [µm]	300.9354	-281.1843	0.06	0.85	4.05 µm	5.31 µm
R_p [µm]	162.1268	-157.2091	0.34	0.91	1.71 µm	3.90 µm
R_{sm} [mm]	1.2324	-1.1371	4231	0.86	0.02 mm	0.02 mm
R_{sk} [-]	11.5163	-13.0721	11.61	0.69	0.29	0.57

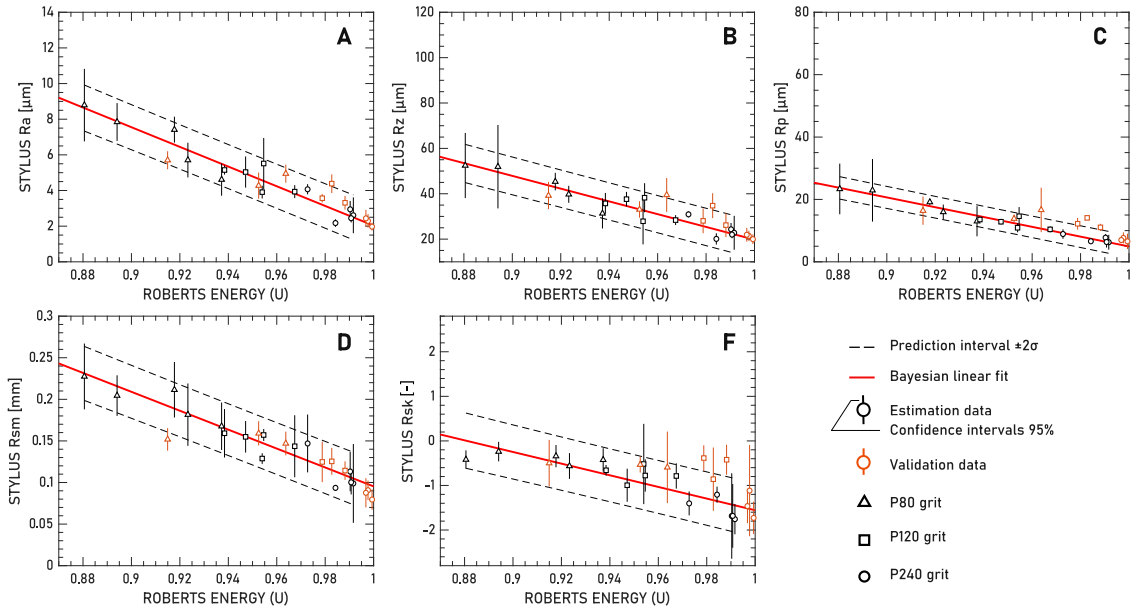

Figure 12. Bayesian linear models relating roughness and features obtained from the GLCM, based on the values of the stylus profilometer.

Similarly to the previous models, Figure 13 shows the models obtained by comparing the vision method with the parameters measured with the confocal microscope. Table 6 gathers the coefficients and evaluations of the proposed models.

Table 6. Coefficients and goodness of fit the models defined by Equation 10, using the confocal microscope.

Roughness Parameter confocal	Interception w_0	Coefficient w_1	Precision β	R^2 estimation	RMSE estimation data	RMSE validation data
R_a [µm]	77.6082	-75.3876	1.55	0.91	0.80 µm	1.43 µm
R_z [µm]	592.2905	-560.8858	0.01	0.83	8.51 µm	12.16 µm
R_p [µm]	404.1223	-390.9245	0.02	0.79	6.84 µm	8.89 µm
R_{sm} [mm]	0.8819	-0.7777	2657	0.65	0.02 mm	0.02 mm
R_{sk} [-]	10.8143	-11.3263	4.77	0.41	0.46	0.53

Again, the Roberts and Uniformity of Energy combination delivered the best models.

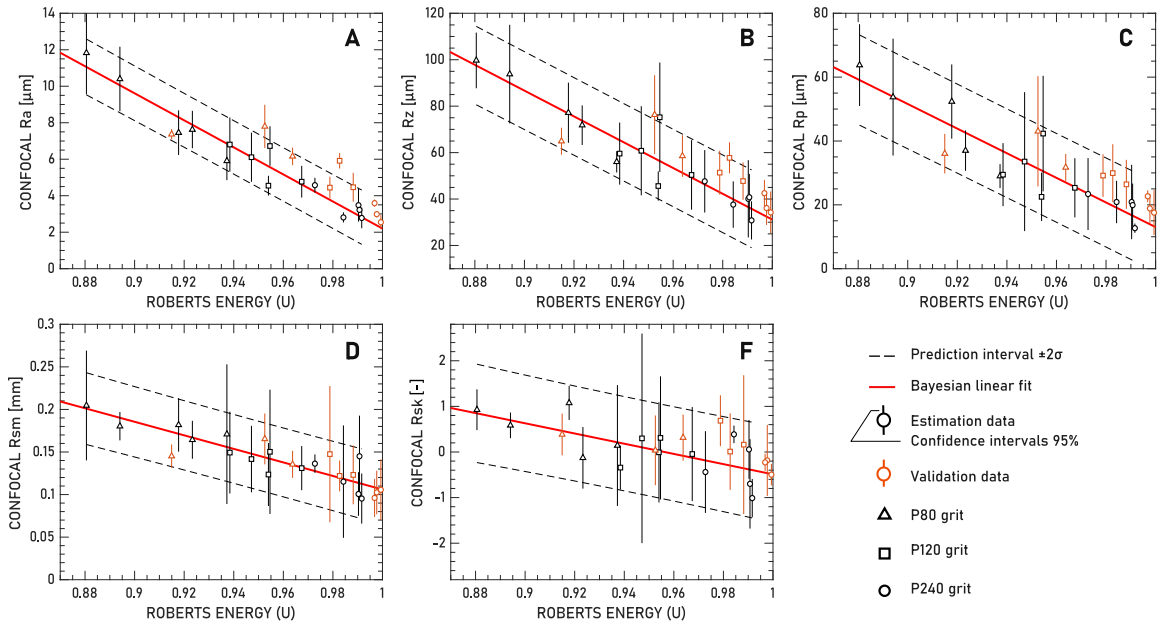

Figure 13. Bayesian linear models relating the roughness and features obtained from the GLCM, based on the values of the confocal microscope.

3.3 Analysis of results

For the developed models, the evaluation of error (RMSE) between each combination of algorithm-feature and surface roughness parameter, shows that the best performance was found in the combination of the Roberts algorithm and the Uniformity of Energy feature; thus, this selection was presented in the results.

Based on the results, the repetition of the same algorithm-feature combinations may be due to the high correlation that the roughness parameters present with each other, as reported in previous investigations [41].

Regarding the evaluation of the models (Equation 10), results showed that the best-evaluated parameter is R_a, and the worst-evaluated is R_{sk}. In general, the proposed method fits better with the measurements made with the stylus profilometer, possibly due to the resolution scales for which each instrument is intended. The confocal microscope is more susceptible to recording variations not recognised by the stylus or the digital image.

To complement the results presented, Table 7 gathers the values of the Ra parameter for the validation workpieces measured using the stylus profilometer, the confocal microscope, and the computer vision system (stylus model). The differences observed at each validation point for the three methods are higher at greater roughness and decrease with lower roughness; this behaviour is expected due to the lack of uniformity in the coarse-grit sandpaper, which generates a higher dispersion of roughness in the surface. Beyond the observed difference, the roughness estimated by the proposed computer vision system is in good agreement with the roughness measured with the stylus profilometer, considered as the standard measuring method. Thus, taking into account that the field of application of this investigation is the manufacturing of wooden parts, we consider that the capacity of the computer vision system to estimate surface roughness is very high.

Table 7. Comparison of Ra obtained with the studied methods.

Validation Workpiece	R_a [µm]		
	Stylus (1)	Confocal (1)	Computer vision (2)
1	4.95 ± 0.51	6.16 ± 0.48	4.02 ± 1.25
2	5.70 ± 0.51	7.37 ± 0.28	6.72 ± 1.25
3	4.27 ± 0.73	7.80 ± 1.18	4.62 ± 1.21
4	4.38 ± 0.52	5.91 ± 0.42	2.97 ± 1.23
5	3.31 ± 0.38	4.46 ± 0.79	2.69 ± 1.27
6	3.57 ± 0.24	4.44 ± 0.60	3.19 ± 1.24
7	2.30 ± 0.38	2.99 ± 0.17	2.14 ± 1.26
8	2.44 ± 0.48	3.59 ± 0.20	2.19 ± 1.26
9	1.97 ± 0.21	2.54 ± 0.39	2.08 ± 1.26

(1) Mean value of three measuring points and its confidence interval.
(2) Estimated value and its prediction interval.

When observing the behaviour followed by the measurements used to validate the models, in most cases, the values obtained are within the prediction band, which implies reproducibility in the results. However, it is crucial to consider, as pointed out by Lu et al. [20], that the models based on GLCM features must be calibrated according to the

material and environmental light conditions, which opens the possibility of carrying out studies related to the optimisation of light conditions according to the material and the operation. Thus, calibration aspects added to the differences in the applied methodology could explain the differences with the results obtained by Ghodrati et al. [15], in which the Laplacian of Gaussian obtained the best results.

The results revealed the enhanced performance of combining the Roberts algorithm and the Uniformity of Energy feature to estimate surface roughness. The Roberts algorithm filters the image using two 2x2 convolution masks, equivalent to the first derivative, generating an enhancement of the intensity changes in the image in two directions, which are then vectorially summed. Compared to the Sobel and Prewitt operators, Roberts is more sensitive to noise, an advantage for roughness estimation. On the other hand, the Laplacian and the Laplacian of Gaussian use a mask that represents the second derivative, generating an enhancement in the local maxima, which is helpful in detecting the edges of a part but not for roughness estimation.

Moreover, the Uniformity of Energy, which corresponds to the sum of the squares of the co-occurrences, is high when there are several repeated pairs in the matrix and low when there are few repeated pairs. As the image was previously enhanced with the Roberts filter and reduced to 8 grey levels, the image of a rougher surface will present a higher variability between pixel pairs, generating a lower number of repeated pairs and, therefore, a low Uniformity of Energy value (a GLCM with low values). In contrast, in an image of a part with low roughness, pixel pairs will repeat more frequently. Due to the few changes of grey levels in the image, the GLCM values will be high in a few matrix elements, resulting in a high Uniformity of Energy. Finally, while Uniformity of Energy showed the best results, Entropy and Contrast operators also gave high goodness of fit (Tables 3 and 4). However, the Uniformity of Energy was chosen because, in addition to its high performance, it was the most straightforward computing characteristic.

Medium-density fibreboards, despite being more homogeneous than other types of wood, exhibit density variations at different depths [6], [29], so it is necessary to study whether the proposed technique is still effective when sanding to greater depths. However, in finishing operations, such as sanding, the depths are less, so the effect of the change in density can be negligible.

The model developed in this study covers sandpaper grit sizes commonly used in the wood products manufacturing industry, considering the goal of automating the inspection

of surface roughness. The roughness values after sanding MDF usually start from Ra = 2 µm upwards. These values are within the typically expected roughness ranges for a wide variety of wood species, as previously reported by Zhong et al. [42].

Regarding the image capture settings, the experiments used a long exposure time, which in some particular cases might be too long to be implemented in real-time surface roughness inspection; however, this is not perceived as a difficulty because it is possible to reduce the exposure time by using better lighting or opening the aperture of the lens. In doing so, the researchers recommend keeping the ISO gain to a minimum so as not to introduce noise into the image, which can confuse the algorithm.

Future work will be to evaluate the performance of the proposed methodology in other areas of the specimen, where sanding marks have different directions due to the nature of the rotary sanding operation; in these cases, it may be necessary to modify the hyperparameters of the co-occurrence matrix, such as the displacement vector and the number of levels to optimise the algorithm's performance. There is an opportunity for future research to focus on optimising lighting conditions and image capture to adapt the algorithms to a specific industrial application that may demand higher shutter speed photographic captures. In addition, it should be tested whether the technique is effective on other wood materials that require sanding operations, such as plywood boards, widely used for furniture manufacturing. In this case, it might be necessary to complement the method for incorporating image processing steps to identify and manage the variations and attributes of natural wood, such as knots and cracks, not present in MDF.

4. Conclusions

This study introduces a novel method for automating the evaluation of surface roughness in wood-based sanded materials through image processing tailored for industrial applications. The investigators established the robustness of the method by applying it to estimate the surface roughness of sanded MDF specimens and calibrating it using Bayesian linear models with measurements from a stylus profilometer and a confocal microscope.

This research validated the suitability of both instruments for characterising sanded MDF surfaces and presented a novel approach: combining an edge detection algorithm with GLCM-based feature extraction, resulting in superior correlations with surface roughness compared to the original image-extracted features. Among all possible algorithm-feature

combinations, the top-performing was Roberts for the edge detection algorithm and Uniformity of Energy for feature extraction, proving the feasibility of estimating sanded MDF roughness using computer vision.

Implementing the method in a computer vision system is an innovative technique for surface roughness estimation in wood-based products, promising enhanced performance in quality control of finishing operations, with potential applications across diverse materials. While the method requires calibration for changing image resolution or lighting conditions, this can be achieved using roughness data from a profilometer or a confocal microscope, as demonstrated in this study. Future research endeavours will expand the scope of these findings to encompass various materials.

Acknowledgements

The authors thank the support of ANID Chile for financing the projects FONDEF IT21i0069 and FONDEF VIU22P0027. The authors also thank the support of 3M Chile for the contribution of sanding discs for the tests, Eng. Pablo Sanhueza for his help in programming the collaborative robot for sanding tests, and Prof. Ricardo Alzugaray for his valuable comments on the manuscript.

Appendix 1

Table 8 presents the convolution masks of the enhancement algorithms and Table 9 the equations for obtaining the GLCM features.

Table 8. Convolution masks used in this research.

Edge detection algorithm	Convolution masks
Roberts	$G_x =$ 1 0 0 -1 $G_y =$ 0 -1 1 0
Sobel	$G_x =$ -1 0 1 -c 0 c -1 0 1 $G_y =$ 1 c 1 0 0 0 -1 -c -1 With c = 2.
Prewitt	Identical to Sobel, but with c = 1.
Laplacian	$\nabla^2 =$ 0 1 0 1 -4 1 0 1 0
Laplacian of Gaussian (*LoG*)	$LoG =$ 0 0 -1 0 0 0 -1 -2 -1 0 -1 -2 16 -2 -1 0 -1 -2 -1 0 0 0 -1 0 0

Table 9. GLCM features.

Feature	Equation
Uniformity of Energy	$U = \sum_{i,j} M_{\mathrm{cn}}^2[i,j]$
Contrast	$C = \sum_{i,j} (i-j)^2 M_{\mathrm{cn}}[i,j]$
Homogeneity	$H = \sum_{i,j} \frac{M_{\mathrm{cn}}[i,j]}{1+\lvert i-j \rvert}$
Autocorrelation	$A = \sum_{i,j} \frac{(i-\mu)(j-\mu)M_{\mathrm{cn}}[i,j]}{\sigma^2}$
Shannon Entropy	$S = -\sum_{i,j} M_{\mathrm{cn}}[i,j] \log(M_{\mathrm{cn}}[i,j])$

Appendix 2

Figure 14 shows the means of each feature algorithm combination for the three grit sizes, with 95% confidence intervals.

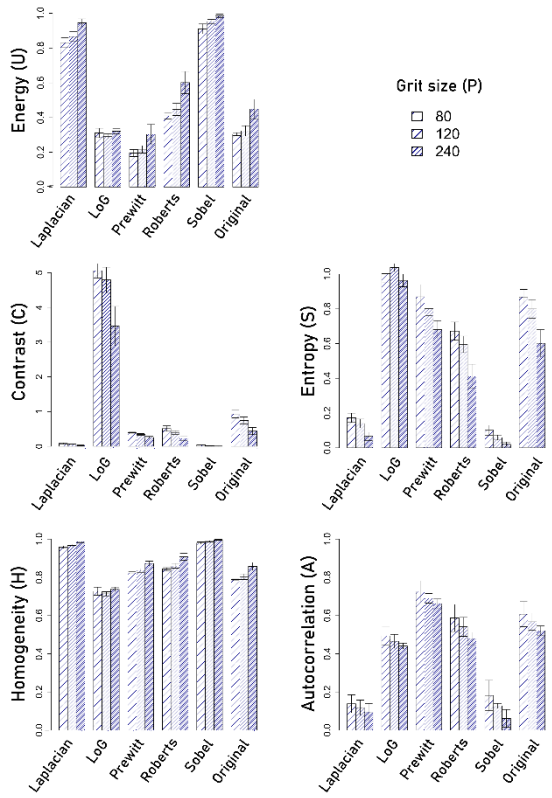

Figure 14: Means of the features extracted from the GLCM for each edge detection algorithm and the original image.

Appendix 3

Table 10 and Table 11 present the mean absolute percentage error (MAPE) for Ra in stylus and confocal models.

Table 10. MAPE for stylus-based models.

	Uniformity of Energy (U)	Entropy (S)	Contrast (C)	Homogeneity (H)	Autocorrelation (A)
Original	0.27	0.24	0.27	0.32	0.41
Roberts	**0.12**	0.14	0.13	0.13	0.39
Sobel	0.37	0.29	0.21	0.29	0.50
Prewitt	0.32	0.28	0.20	0.28	0.46
Laplacian	0.20	0.21	0.19	0.20	0.32
LoG	0.47	0.39	0.31	0.46	0.53

Table 11. MAPE for confocal-based models.

	Uniformity of Energy (U)	Entropy (S)	Contrast (C)	Homogeneity (H)	Autocorrelation (A)
Original	0.29	0.25	0.30	0.34	0.37
Roberts	**0.16**	0.17	0.16	0.17	0.43
Sobel	0.36	0.31	0.23	0.30	0.55
Prewitt	0.33	0.30	0.23	0.29	0.51
Laplacian	0.23	0.25	0.23	0.23	0.35
LoG	0.47	0.38	0.34	0.45	0.58

References

[1] E. Diez Cifuentes, R. Alzugaray Franz, A. Padilla Bernedo, E. Leal Muñoz, and M. Madaf Poblete, “Robotized workstation for intelligent sanding processes of wooden workpieces,” *DYNA*, vol. 98, no. 4, pp. 362–368, 2023, doi: 10.6036/10873.

[2] P. L. Tan, S. Sharif, and I. Sudin, “Roughness models for sanded wood surfaces,” *Wood Sci. Technol.*, vol. 46, no. 1–3, pp. 129–142, 2012, doi: 10.1007/s00226-010-0382-y.

[3] G. Sinn, J. Sandak, and T. Ramananantoandro, “Properties of wood surfaces - Characterisation and measurement. A review. COST Action E35 2004-2008: Wood machining - Micromechanics and fracture,” *Holzforschung*, vol. 63, no. 2, pp. 196–203, 2009, doi: 10.1515/HF.2009.016.

[4] L. Gurau and M. Irle, “Surface Roughness Evaluation Methods for Wood Products: a Review,” *Curr. For. Reports*, vol. 3, no. 2, pp. 119–131, 2017, doi: 10.1007/s40725-017-0053-4.

[5] E. Csanády and E. Magoss, *Mechanics of Wood Machining*. Berlin, Heidelberg: Springer Berlin Heidelberg, 2013.

[6] A. Aguilera, “Surface roughness evaluation in medium density fibreboard rip sawing,” *Eur. J. Wood Wood Prod.*, vol. 69, no. 3, pp. 489–493, 2011, doi: 10.1007/s00107-010-0481-3.

[7] E. Magoss, R. Rozs, and S. Tatai, “Evaluation of Wood Surface Roughness by Confocal Microscopy,” *Wood Res.*, vol. 67, no. 6, pp. 919–928, Dec. 2022, doi: 10.37763/wr.1336-4561/67.6.919928.

[8] J. Caja García, A. Sanz Lobera, P. Maresca, T. Fernández Pareja, and C. Wang, “Some considerations about the use of contact and confocal microscopy methods in surface texture measurement,” *Materials (Basel).*, vol. 11, no. 8, 2018, doi: 10.3390/MA11081484.

[9] Y. Liu, L. Guo, H. Gao, Z. You, Y. Ye, and B. Zhang, “Machine vision based condition monitoring and fault diagnosis of machine tools using information from machined surface texture: A review,” *Mech. Syst. Signal Process.*, vol. 164, no. April 2021, p. 108068, 2022, doi: 10.1016/j.ymssp.2021.108068.

[10] Z. W. Zhong, “Surface roughness of machined wood and advanced engineering materials and its prediction: A review,” *Adv. Mech. Eng.*, vol. 13, no. 5, pp. 1–19, 2021, doi: 10.1177/16878140211017632.

[11] J. Ma *et al.*, “Surface roughness detection based on image analysis,” in *ACM International Conference Proceeding Series*, Jul. 2021, pp. 196–200, doi: 10.1145/3478905.3478945.

[12] R. Kumar, P. Kulashekar, B. Dhanasekar, and B. Ramamoorthy, “Application of digital image magnification for surface roughness evaluation using machine vision,” *Int. J. Mach. Tools Manuf.*, vol. 45, no. 2, pp. 228–234, 2005, doi: 10.1016/j.ijmachtools.2004.07.001.

[13] A. Rolleri and E. Roffael, “Rugosidad de tableros de fibra de densidad media (MDF) usando método de contacto y no contacto,” *Bosque (Valdivia)*, vol. 27, no. 1, pp. 72–77, 2006, doi: 10.4067/s0717-92002006000100009.

[14] M. Nakamura, Y. Kikuchi, S. Hotta, Y. Fujiwara, and T. Konoike, "Evaluation of the sensory roughness of some coated wood surfaces by image analysis," *Eur. J. Wood Wood Prod.*, vol. 76, no. 6, pp. 1571–1580, 2018, doi: 10.1007/s00107-018-1342-8.

[15] S. Ghodrati, M. Mohseni, and S. Gorji Kandi, "Application of image edge detection methods for precise estimation of the standard surface roughness parameters: Polypropylene/ethylene-propylene-diene-monomer blend as a case study," *Meas. J. Int. Meas. Confed.*, vol. 138, pp. 80–90, 2019, doi: 10.1016/j.measurement.2019.02.033.

[16] J. Lu, G. Hu, J. Xia, and Z. Song, "Applications of the Image Processing Technology in Casting Surface Roughness Detection Technology," *J. Phys. Conf. Ser.*, vol. 1748, no. 4, 2021, doi: 10.1088/1742-6596/1748/4/042004.

[17] V. Koblar and B. Filipič, "Evolutionary design of a system for online surface roughness measurements," *Mathematics*, vol. 9, no. 16, pp. 1–18, 2021, doi: 10.3390/math9161904.

[18] Ş. Kilinçarslan, Y. Şimşek Türker, and M. İnce, "Prediction of Heat-Treated Spruce Wood Surface Roughness with Artificial Neural Network and Random Forest Algorithm," *Lect. Notes Data Eng. Commun. Technol.*, vol. 76, pp. 439–445, 2021, doi: 10.1007/978-3-030-79357-9_43.

[19] E. S. Gadelmawla, "A vision system for surface roughness characterization using the gray level co-occurrence matrix," *NDT E Int.*, vol. 37, no. 7, pp. 577–588, 2004, doi: 10.1016/j.ndteint.2004.03.004.

[20] R.-S. Lu, G. Y. Tian, D. Gledhill, and S. Ward, "Grinding surface roughness measurement based on the variogram of speckle pattern texture," *Appl. Opt.*, vol. 45, no. 35, pp. 8839–8847, 2006, doi: 0003-6935/06/358839-09.

[21] K. Joshi and B. Patil, "Evaluation of Surface Roughness by Machine Vision Using Neural Networks Approach," in *Recent Advances in Mechanical Infrastructure, Proceedings of ICRAM 2019*, J. Kacprzyk, Ed. Warszawa, Poland: Springer, 2020, pp. 25–31.

[22] V. Kumar and C. P. Sudheesh Kumar, "Investigation of the influence of coloured illumination on surface texture features: A Machine vision approach," *Meas. J. Int. Meas. Confed.*, vol. 152, p. 107297, 2020, doi: 10.1016/j.measurement.2019.107297.

[23] A. P. Rifai, H. Aoyama, N. H. Tho, S. Z. Md Dawal, and N. A. Masruroh, "Evaluation of turned and milled surfaces roughness using convolutional neural network," *Meas. J. Int. Meas. Confed.*, vol. 161, p. 107860, 2020, doi: 10.1016/j.measurement.2020.107860.

[24] A. Giusti, M. Dotta, U. Maradia, M. Boccadoro, L. M. Gambardella, and A. Nasciuti, "Image-based measurement of material roughness using machine learning techniques," *Procedia CIRP*, vol. 95, pp. 377–382, 2020, doi: 10.1016/j.procir.2020.02.292.

[25] A. P. Rifai, R. Fukuda, and H. Aoyama, "Surface Roughness Estimation and Chatter Vibration Identification Using Vision-Based Deep Learning," *J. Japan Soc. Precis. Eng.*, vol. 85, no. 7, pp. 658–666, Jul. 2019, doi: 10.2493/jjspe.85.658.

[26] L. Lu, H. Yi, A. Shu, J. Qin, and E. Lu, "Deep learning classification and recognition

method for milling surface roughness combined with simulation data," *Metrol. Meas. Syst.*, vol. 30, no. 1, pp. 117–138, 2023, doi: 10.24425/mms.2023.144401.

[27] B. Bhandari, G. Park, and N. Shafiabady, "Implementation of transformer-based deep learning architecture for the development of surface roughness classifier using sound and cutting force signals," *Neural Comput. Appl.*, vol. 35, no. 18, pp. 13275–13292, 2023, doi: 10.1007/s00521-023-08425-z.

[28] C. He, J. Yan, S. Wang, S. Zhang, G. Chen, and C. Ren, "A theoretical and deep learning hybrid model for predicting surface roughness of diamond-turned polycrystalline materials," *Int. J. Extrem. Manuf.*, vol. 5, no. 3, p. 035102, 2023, doi: 10.1088/2631-7990/acdb0a.

[29] M. Farajollah Pour, H. Hatefnia, A. Dorieh, M. Valizadeh Kiamahalleh, and Y. Mohammadnia Afrouzi, "Research on Medium density fiberboard (MDF) behavior against screw axial withdrawal: Impact of density and operational variables," *Structures*, vol. 39, no. March, pp. 194–206, 2022, doi: 10.1016/j.istruc.2022.03.025.

[30] W. P. Dong, P. J. Sullivan, and K. J. Stout, "Comprehensive study of parameters for characterising three- dimensional surface topography. III: Parameters for characterising amplitude and some functional properties," *Wear*, vol. 178, no. 1–2, pp. 29–43, 1994, doi: 10.1016/0043-1648(94)90127-9.

[31] ISO 21920-2:2021(en), "Geometrical product specifications (GPS) — Surface texture: Profile — Part 2: Terms, definitions and surface texture parameters." International Organization for Standardization, 2021, [Online]. Available: https://www.iso.org/standard/72226.html.

[32] J. Seewig, P. J. Scott, M. Eifler, B. Barwick, and D. Hüser, "Crossing - The-line segmentation as a basis for Rsm and Rc evaluation," *Surf. Topogr. Metrol. Prop.*, vol. 8, no. 2, 2020, doi: 10.1088/2051-672X/ab958c.

[33] A. Piratelli-Filho, G. H. Sternadt, and R. V. Arencibia, "Removing deep valleys in roughness measurement of soft and natural materials with mathematical filtering," *Cienc. y Eng. Sci. Eng. J.*, vol. 21, no. 2, pp. 29–34, 2012, doi: 10.14393/19834071.2012.13669.

[34] The MathWorks Inc., "MATLAB." The MathWorks Inc., Natick, Massachusetts, United States, 2023, [Online]. Available: https://www.mathworks.com.

[35] Digital Surf, "MountainsLab Premium." Digital Surf, Besançon, France, 2023, [Online]. Available: https://www.digitalsurf.com.

[36] R. Jain, R. Kasturi, and B. Schunck, *Machine Vision*. McGraw-Hill, Inc, 1995.

[37] R. M. Haralick, I. Dinstein, and K. Shanmugam, "Textural Features for Image Classification," *IEEE Trans. Syst. Man Cybern.*, vol. SMC-3, no. 6, pp. 610–621, 1973, doi: 10.1109/TSMC.1973.4309314.

[38] R. M. Haralick and L. G. Shapiro, *Computer and Robot Vision*, First Edit., vol. 1. Addison-Wesley Publishing Company, 1992.

[39] C. M. Bishop, *Pattern Recognition and Machine Learning*. Springer Berlin Heidelberg, 2006.

[40] F. Iglesias, A. Aguilera, A. Padilla, A. Vizán, E. Diez, Dataset: Robotic Sanding MDF Roughness, Figshare (2023), https://doi.org/10.6084/m9.figshare.24116583.v1.

[41] O. A. Gorlenko, “Assessment of surface roughness parameters and their interdependence,” *Precis. Eng.*, vol. 3, no. 2, pp. 105–108, 1981, doi: 10.1016/0141-6359(81)90045-3.

[42] Z. W. Zhong, S. Hiziroglu, and C. T. M. Chan, “Measurement of the surface roughness of wood based materials used in furniture manufacture,” *Measurement*, vol. 46, no. 4, pp. 1482–1487, 2013, doi: https://doi.org/10.1016/j.measurement.2012.11.041.